

Experimental Demonstration of Frequency Regulation by Commercial Buildings – Part I: Modeling and Hierarchical Control Design

Evangelos Vrettos^{*1}, Emre C. Kara^{†2}, Jason MacDonald^{‡3},
Göran Andersson^{§1}, and Duncan S. Callaway^{¶4}

¹Power Systems Laboratory, ETH Zurich, Switzerland

²National Accelerator Laboratory (SLAC), California, US

³Grid Integration Group, Lawrence Berkeley National Laboratory (LBNL),
California, US

⁴Energy and Resources Group, University of California, Berkeley, US

May 20, 2016

Abstract

This paper is the first part of a two-part series in which we present results from an experimental demonstration of frequency regulation in a commercial building test facility.

In Part I, we introduce the test facility and develop relevant building models. Furthermore, we design a hierarchical controller that consists of three levels: a reserve scheduler, a building climate controller, and a fan speed controller for frequency regulation. We formulate the reserve scheduler as a robust optimization problem and introduce several approximations to reduce its complexity. The building climate controller is comprised of a robust model predictive controller and a Kalman filter. The frequency regulation controller consists of a feedback and a feedforward loop, provides fast responses, and is stable.

Part I presents building model identification and controller tuning results, whereas Part II reports results from the operation of the hierarchical controller under frequency regulation.

*vrettos@eeh.ee.ethz.ch

†eckara@slac.stanford.edu

‡jmacdonald@lbl.gov

§andersson@eeh.ee.ethz.ch

¶dcal@berkeley.edu

Acronyms

AHU	Air Handling Unit
AS	Ancillary Service
BAS	Building Automation System
CWS	Central Working Station
FLEXLAB	Facility for Low Energy eXperiments
HVAC	Heating, Ventilation and Air-Conditioning
MPC	Model Predictive Control
PI	Proportional-Integral
PID	Proportional-Integral-Derivative
PJM	Pennsylvania, Jersey, and Maryland Power Market
RES	Renewable Energy Source
RMSE	Root Mean Squared Error
SAT	Supply Air Temperature
TSO	Transmission System Operator
VAV	Variable Air Volume
VFD	Variable Frequency Drive

1 Introduction

1.1 Motivation and Related Work

Power system frequency reflects the balance between generation and demand of electric power. If generation exactly meets demand, the frequency is at its nominal value (50 Hz in Europe and 60 Hz in North America). On the other hand, if generation becomes lower than demand, the frequency drops and vice versa. Transmission System Operators (TSOs) rely on frequency control reserves in the form of Ancillary Services (AS) to stabilize frequency after a sudden disturbance and recover it to its nominal value.

The integration of fluctuating Renewable Energy Sources (RES) in the grid increases the need for frequency control reserves [1]. Although these reserves are traditionally provided by power plants, additional reserve resources will be needed with large RES shares. Conceptually, loads can provide frequency control

by reducing their consumption when frequency is low and increasing consumption when frequency is high [2].

Heating, Ventilation and Air-Conditioning (HVAC) systems in commercial buildings are well suited for frequency control for three main reasons: (i) commercial HVAC systems make up a large percentage of the total electricity demand of a country (around 20% in the US [3,4]), (ii) commercial buildings often have a large thermal inertia, and (iii) many buildings (one-third of all buildings in the US [3]) have a Building Automation System (BAS) that facilitates control implementation. However, HVAC systems are typically complex with many control variables and cascaded control loops. Most of the early work on commercial buildings focused on the development of building thermal models [5,6], and on using the building's thermal mass for load shifting and peak shedding to minimize electricity cost and demand charges [7–9].

Some works investigated the potential of commercial buildings for AS provision. A retail store and an office building participated in a pilot program for non-spinning reserves in the California Independent System Operator's AS market using global temperature adjustments in [10]. In [11] spinning reserve with a duration of 15 minutes was successfully offered by curtailing the air conditioning load of a hotel. Ref. [12] used a detailed model of a Variable Air Volume (VAV) HVAC system to simulate the provision of spinning reserve with setpoint adjustments in zone temperature, duct static pressure, Supply Air Temperature (SAT), and chilled water temperature.

This paper concerns frequency regulation from commercial buildings, which is also known as secondary (or load) frequency control, automatic generation control, and frequency restoration reserve. Frequency regulation is activated via a signal sent from the TSO typically every 2 – 4 seconds with the goal of correcting frequency and tie-line power deviations [13]. There is a limited amount of theoretical, simulation-based or experimental work on frequency regulation with commercial buildings. In [14] a heat pump was controlled to track a frequency regulation signal by changing the refrigerant's flow rate. Adjustments of the duct static pressure setpoint were used in a simulation study in [15] for frequency regulation. Refs. [3] and [16] investigated frequency regulation via fan power control and simulations showed that 15% of the fan power can be offered as reserve, when the frequency band of the regulation signal is $f \in [1/(10 \text{ min}), 1/(4 \text{ sec})]$. The follow-up work [17] included chiller control enlarging the frequency band to $1/(60 \text{ min})$.

Since buildings are energy-constrained resources it is important to determine the reserve capacity reliably. Model Predictive Control (MPC) was used in [18] to quantify the flexibility of a commercial building and offer it to a utility. Ref. [19] presented a hierarchical control framework consisting of a reserve capacity scheduler, an MPC for HVAC system control, and a feedback controller to track the regulation signal. The framework of [19] was extended in [20] to include energy-constrained regulation signals, and in [21] with a chance-constrained reserve scheduling formulation. Ref. [22] proposed a simulation-based approach to

estimate the reserve capacity neglecting the time-coupling across different scheduling intervals. The energy capacity of a commercial building was estimated in [23] with a virtual battery model.

Estimating the building’s baseline consumption without frequency regulation is challenging. Baseline estimation was performed on-line in [24] using a low-pass filter. If MPC is used as in [18–21] the baseline power is known ahead of time, which is advantageous because it facilitates the financial settlement.

Apart from simulation-based studies, experimental verification of frequency regulation by commercial buildings is necessary to build confidence for widespread implementation. Unfortunately, there have been only a few demonstrations and field tests so far. The feasibility of offering up- and down-regulation products with global temperature adjustments and ventilation power control was investigated in [25]. Ref. [26] demonstrated that fans can provide frequency regulation with open-loop control of the frequency of the Variable Frequency Drive (VFD) using industry-standard demand response communications. In [24] an auditorium of a university building provided frequency regulation controlling the fan speed and air flow rate setpoints. The fan power was indirectly controlled via static duct pressure setpoint adjustments in [18].

Frequency regulation experiments with a variable speed heat pump were reported in [27] in a lab-scale microgrid, using direct compressor control and adjustments of the supply water temperature setpoint. Ref. [28] developed a Proportional-Integral-Derivative (PID) controller for frequency regulation with a chiller, and combined it with a high-pass filter of the regulation signal and a baseline estimator. The follow-up work [29] identified the BAS delays and chiller ramp-rates and minimum cooling power limits as important issues for practical implementation. Finally, [30] investigated experimentally the efficiency of fast demand response actions in commercial buildings.

1.2 Contribution and Organization of this Paper

To the best of our knowledge, this two-part paper presents the first experimental demonstration of frequency regulation from a commercial building that simultaneously addresses the following challenges: (i) a priori determination of reserve capacity and bidding in a day-ahead AS market; (ii) a priori declaration of the short-term operating power around which we provide frequency regulation; (iii) balancing energy consumption and reserve capacity, such that the net profit is maximized and the effect on occupant comfort is minimal; and (iv) accurate tracking of the regulation signal with fan speed control.

To this end, we adopt the hierarchical control framework of [19–21] and extend it in several ways. We determine the reserve capacity in a day-ahead fashion using robust optimization, and control the HVAC system with a robust MPC. In contrast to [19–21], we investigate the use of different building models in the reserve scheduler and MPC controller, and develop a Kalman filter to provide state estimates to the controller. Whereas [19–21] considered water-based HVAC sys-



Figure 1: The Facility for Low Energy eXperiments (FLEXLAB) at LBNL.

tems, we focus on VAV HVAC systems with fans and propose computationally tractable reformulations to account for the fan nonlinear dynamics. Furthermore, in contrast to [26] that used open-loop control and to [24] that developed a standard Proportional-Integral (PI) controller for the fan, we propose a switched controller with a feedforward and a feedback loop in order to track the regulation signal. The proposed controller demonstrates a high performance without compromising stability.

In Part I of this two-part paper, we introduce the test facility in Section 2, identify simple building models in Section 3, and present the hierarchical control design in Sections 4 - 6. Extensive experimental results are reported in Part II [31].

2 Test Facility

2.1 FLEXLAB: our Test Facility

The experiment was performed at the Facility for Low Energy eXperiments (FLEXLAB), a new facility for energy efficiency research in buildings located at the Lawrence Berkeley National Laboratory (LBNL). The facility (shown in Fig. 1) is comprised of 4 buildings (called “bays”) and each of them has 2 thermally isolated test “cells”. Each pair of cells is designed to be thermally identical, constructed with the same materials and dimensions.

The thermal isolation resulting from the near adiabatic walls between the two cells allows them to be modeled independently. This is a unique feature of FLEXLAB that allows us to perform frequency regulation experiments in one of the two identical cells (cell “1A”), while using the other one (cell “1B”) as a benchmark to evaluate the effect of our control actions in real time and under the same external conditions. The bay used in our experiment has a south orientation and a total floor area of 120 m^2 (60 m^2 per building cell).

Three major cascade control loops are present in a VAV HVAC system: chilled water temperature control, SAT control, and zone (room) temperature control. A chiller plant cools down water that is then piped to the building’s Air Handling Unit (AHU). The chilled water decreases the temperature of a mixture of return

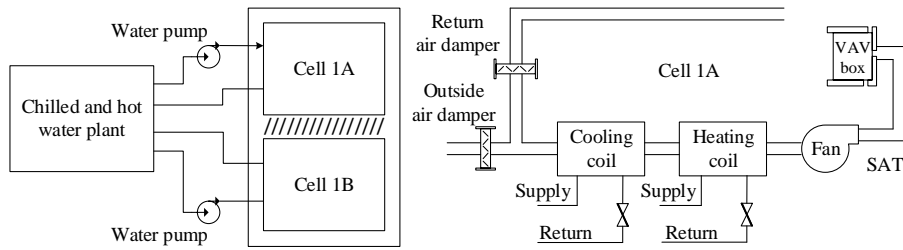


Figure 2: The HVAC system of building cells 1A and 1B of FLEXLAB.

and outside air in the AHU using a heat exchanger, and the flow of the chilled water is controlled to maintain a constant SAT. The cooled air is circulated to the building zones through the duct system using a fan. The temperature of each zone is maintained close to the desired setpoint by controlling the damper position of the VAV box.

Typically, an AHU provides several building zones with cooled air, whereas reheating is performed at the VAV boxes. As shown in Fig. 2, FLEXLAB differs from this typical mode of operation in two ways: (i) the cells are served by dedicated AHUs that contain a heating coil; and (ii) the air volume is controlled by fan speed alone rather than damper position. Although small, the test facility is a good representation of commercial buildings with VAV systems constructed in the 1980's and is highly controllable.

2.2 Control Approach

FLEXLAB is controlled by a Central Working Station (CWS) based on an existing control sequence programmed in LabVIEW. From a TestStand National Instruments user interface, the operator can monitor the system and modify the setpoints of various control loops. We develop the hierarchical controller for frequency regulation externally in order to minimize potential conflicts with the LabVIEW code, and send the control commands to the CWS via a scripting environment.

Specifically, we disable the zone temperature PI control of FLEXLAB and replace it with an MPC-based controller, which determines the air flow rate setpoints. However, the hierarchical controller does not substitute the chilled water temperature and SAT control loops of the HVAC system, which remain active. The hierarchical controller consists of the following three levels, and the control sequences are shown in Fig. 3.

2.2.1 Level 1: Reserve Scheduler

The goal of the reserve scheduler is to determine the reserve capacity that the building can reliably offer to the TSO by solving a multi-period robust optimization problem. We assume a day-ahead reserve scheduling occurring at 12.00 of each

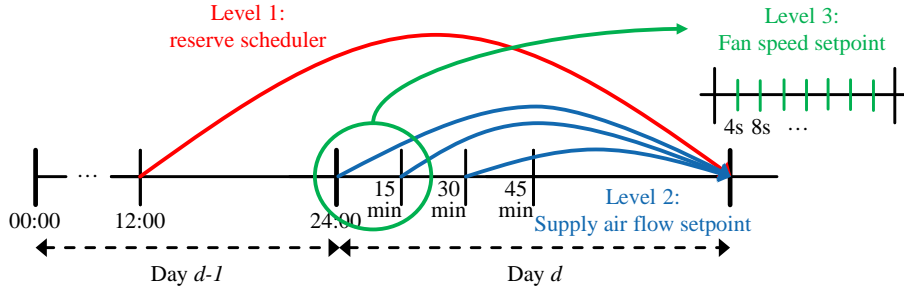


Figure 3: Control sequences of the three levels of the hierarchical controller.

day to determine the reserve capacity for the next day, which is common in several AS markets [32].

2.2.2 Level 2: Room Climate Controller

This zonal controller calculates the supply air flow rate setpoints that minimize energy consumption while ensuring occupant comfort under reserve provision. It is implemented as a robust MPC that runs every 15 minutes along with a Kalman filter.

2.2.3 Level 3: Frequency Regulation Controller

The goal of this controller is to track the frequency regulation signal every 4 seconds by modifying the fan power via fan speed control with a VFD. For this purpose, we designed a switched controller comprised of a feedforward model-based controller and a feedback PI controller.

3 Modeling and Identification

3.1 Building Thermal Model

We model the building with the 2-state resistance-capacitance network of Fig. 4. If the heating coil of the AHU is deactivated, the cooling power of the HVAC system is given by $Q_c = \dot{m}c_p(T_s - T_r)$, where T_r is the room temperature, \dot{m} is the mass air flow rate, c_p is the specific heat capacity of air, and T_s is the SAT. Let us denote by: T_m the temperature of the building's lumped thermal mass; C_r and C_m the thermal capacitances of the room and the thermal mass; T_a the ambient temperature; R_{ra} and R_{rm} the thermal resistances between the room and the ambient, and between the room and the thermal mass, respectively; G the solar irradiance; γ the solar irradiance absorption factor; and I_g the internal heat gain. With this notation, the

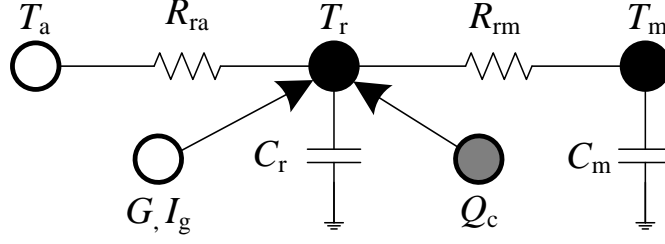


Figure 4: The resistance-capacitance network of the building thermal model.

continuous-time state-space model can be written as

$$\begin{aligned}
 \begin{bmatrix} \dot{T}_r \\ \dot{T}_m \end{bmatrix} &= \overbrace{\begin{bmatrix} -\left(\frac{1}{C_r R_{ra}} + \frac{1}{C_r R_{rm}}\right) & \frac{1}{C_r R_{rm}} \\ \frac{1}{C_m R_{rm}} & -\frac{1}{C_m R_{rm}} \end{bmatrix}}^{A^c} \cdot \begin{bmatrix} T_r \\ T_m \end{bmatrix} + \overbrace{\begin{bmatrix} \frac{c_p T_s}{C_r} \\ 0 \end{bmatrix}}^{B_u^c} \dot{m} + \\
 &\overbrace{\begin{bmatrix} -\frac{c_p}{C_r} & 0 \\ 0 & 0 \end{bmatrix}}^{B_{xu}^c} \cdot \begin{bmatrix} T_r \\ T_m \end{bmatrix} \dot{m} + \overbrace{\begin{bmatrix} \frac{1}{C_r R_{ra}} & \frac{\gamma}{C_r} & \frac{1}{C_r} \\ 0 & 0 & 0 \end{bmatrix}}^{B_v^c} \cdot \begin{bmatrix} T_a \\ G \\ I_g \end{bmatrix}. \quad (1)
 \end{aligned}$$

The model is bilinear between the control input \dot{m} and the state T_r . Note that there is no bilinearity between \dot{m} and T_s because T_s is fixed in our experiment.

With a first-order Euler discretization, the discrete-time model maintains the structure of the continuous-time matrices [33]

$$\begin{aligned}
 \begin{bmatrix} T_{r,k+1} \\ T_{m,k+1} \end{bmatrix} &= \overbrace{\begin{bmatrix} a_{11} & a_{12} \\ a_{21} & a_{22} \end{bmatrix}}^A \cdot \begin{bmatrix} T_{r,k} \\ T_{m,k} \end{bmatrix} + \overbrace{\begin{bmatrix} b T_s \\ 0 \end{bmatrix}}^{B_u} \dot{m}_k + \\
 &\overbrace{\begin{bmatrix} -b & 0 \\ 0 & 0 \end{bmatrix}}^{B_{xu}} \cdot \begin{bmatrix} T_{r,k} \\ T_{m,k} \end{bmatrix} \dot{m}_k + \overbrace{\begin{bmatrix} d_{11} & d_{12} & d_{13} \\ 0 & 0 & 0 \end{bmatrix}}^{B_v} \cdot \begin{bmatrix} T_{a,k} \\ G_k \\ I_{g,k} \end{bmatrix}, \quad (2)
 \end{aligned}$$

where the state, input and disturbance vectors are defined as

$$x_k = [T_{r,k} \ T_{m,k}]^\top, \quad u_k = \dot{m}_k, \quad v_k = [T_{a,k} \ G_k \ I_{g,k}]^\top. \quad (3)$$

We developed the following regression problem to identify the entries of matrices A , B_u , B_{xu} , and B_v using measurements of $T_{r,k}$, \dot{m}_k , $T_{a,k}$, G_k , and $I_{g,k}$

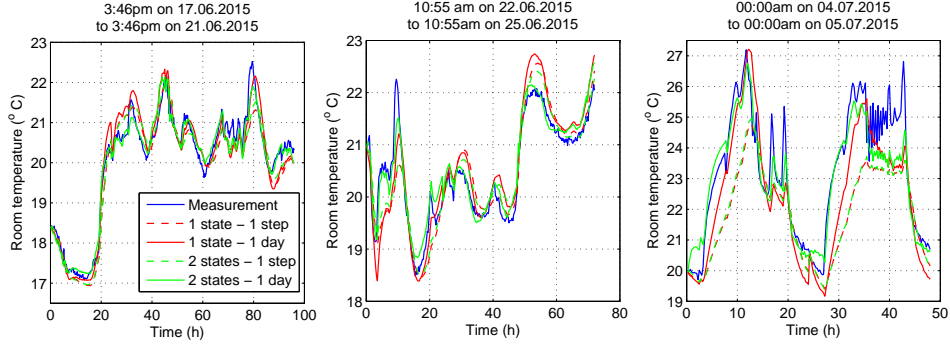


Figure 5: Identification and comparison of four building thermal models.

$$\min_{A, B_u, B_{xu}, B_v, \hat{x}_k} \sum_k [\hat{x}_k(1) - x_k(1)]^2 \quad (4a)$$

$$\text{s.t. } \hat{x}_{k+1} = A x_k + B_u u_k + B_{xu} x_k u_k + B_v v_k, \forall k \quad (4b)$$

$$a_{12}, a_{21}, b, d_{11}, d_{12}, d_{13} \geq 0 \quad (4c)$$

$$\hat{T}_{m,k}^{\min} \leq \hat{x}_k(2) \leq \hat{T}_{m,k}^{\max}, \forall k \quad (4d)$$

$$|\text{eig}(A)| \leq 1, |\text{eig}(A + B_{xu} u_k)| \leq 1, \forall k, \quad (4e)$$

where $x_k(1) = T_{r,k}$ and $x_k(2) = T_{m,k}$. Since the state $T_{m,k}$ is not directly measured, the regression (4) is a non-linear optimization problem that involves multiplications of the optimization variables (the model parameters).

Constraints (4c) represent the fact that the positive elements of the continuous-time matrices A^c , B_u^c , and B_v^c in (1) remain positive in the discrete-time matrices A , B_u , and B_v due to the first-order discretization. Indeed, the discrete-time matrices are computed with $A = I + \Delta t \cdot A^c$, $B_u = \Delta t \cdot B_u^c$, and $B_v = \Delta t \cdot B_v^c$, where $\Delta t = 15$ minutes is the discretization step and I is the identity matrix. Constraints (4d) are lower and upper bounds on the estimated unmeasured state $\hat{x}_k(2) = \hat{T}_{m,k}$ (the bounds $\hat{T}_{m,k}^{\min} = 0.01 \cdot T_{r,k}$ and $\hat{T}_{m,k}^{\max} = 2.5 \cdot T_{r,k}$ were used). Constraints (4e) impose stability of the identified bilinear model to avoid overfitting if the data set is small or if it does not have sufficient excitation in terms of control inputs.

Table 1: Comparison of building models with respect to RMSE

	1 state, 1 step	1 state, 1 day	2 states, 1 step	2 states, 1 day
RMSE	0.92°C	0.67°C	0.89°C	0.42°C

The optimization problem (4) identifies a model based on “1-step ahead prediction” meaning that the estimate $\hat{x}_{k+1}(1) = \hat{T}_{r,k+1}$ at time step $k + 1$ depends directly on the measurement $x_k(1) = T_{r,k}$ at time step k . This model identification approach is standard for MPC applications because the one-step prediction is

Table 2: Parameters of the older model (2 states, 1 day prediction)

$a_{11} = 0.8665$	$a_{12} = 0.0918$	$a_{21} = 0.0374$	$a_{22} = 0.9703$
$b = 0.2996$	$d_{11} = 0.0230$	$d_{12} = 2.016 \cdot 10^{-4}$	$d_{13} = 1.424 \cdot 10^{-4}$

Table 3: Parameters of the new model (2 states, 1 day prediction)

$a_{11} = 0.6344$	$a_{12} = 0.2661$	$a_{21} = 0.1021$	$a_{22} = 0.9170$
$b = 0.4716$	$d_{11} = 0.0405$	$d_{12} = 0.0028$	$d_{13} = 3.3686 \cdot 10^{-4}$

Table 4: Fan model parameters

$\alpha_3 = 2588.2$	$\alpha_2 = -1458.0$	$\alpha_1 = 630.9$	$\alpha_0 = 28.7$
$\beta_3 = 0.0032$	$\beta_2 = -0.0151$	$\beta_1 = 1.4521$	$\beta_0 = 55.7634$
-	-	$\gamma_1 = 0.0133$	$\gamma_0 = 0.0606$

important. Nevertheless, in this experiment the building model is also used in the reserve scheduler, and thus high-quality day-ahead predictions are also important.

For this purpose, we propose to modify the regression problem by substituting the measurement $x_k(1) = T_{r,k}$ with the optimization variable $\hat{x}_k(1) = \hat{T}_{r,k}$ in (4b). We use this more complex formulation to obtain a “1-day ahead prediction” model, which is expected to predict the building states up to one day ahead more accurately, because it is more flexible than the original formulation. Of course, it is also possible to identify a 1st-order model by neglecting the lumped thermal mass of the room, which simplifies the regression problem significantly.

Two sets of building model parameters were fitted to investigate the importance of periodic calibration. The first set (“older model”) used data from 17 – 25 June and 4 – 5 July 2015, whereas the second set (“new model”) used data from 12 – 18 November 2015. The building was excited with different combinations of air flow rate, SAT, and internal heat gains. Four different model variants were compared: (i) 1-state model with 1-step ahead prediction, (ii) 1-state model with 1-day ahead prediction, (iii) 2-state model with 1-step ahead prediction, and (iv) 2-state model with 1-day ahead prediction.

The identification results are shown in Fig. 5 and the model Root Mean Squared Errors (RMSEs) are given in Table 1. As expected, increasing the number of states or the prediction horizon reduces the RMSE. We use the 2-state model with 1-day ahead prediction in the frequency regulation experiments because it achieves the lowest RMSE. The identified model parameters are shown in Tables 2 and 3.

3.2 Fan Model

A steady-state fan model is required in the MPC to map the air flow setpoint to fan power, and in the frequency regulation controller to convert the electric power setpoint to a fan speed reference. According to the fan laws, the mass air flow rate

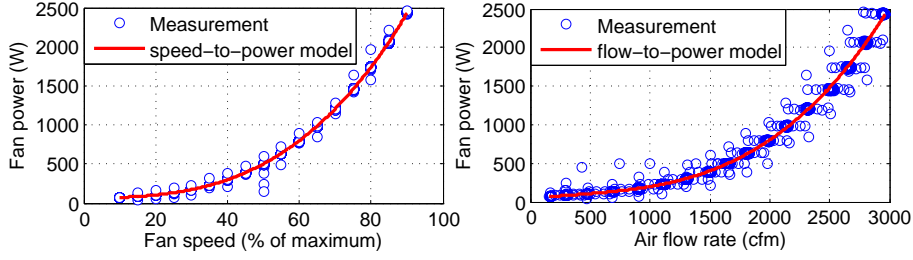


Figure 6: Raw fan measurements and the identified fan models.

u is proportional to the fan speed N_f , and the fan power P_f increases with the cube of the fan speed. Therefore, a steady-state model can be obtained by fitting the parameters of

$$P_f = f(u) = \alpha_3 u^3 + \alpha_2 u^2 + \alpha_1 u + \alpha_0 \quad (5)$$

$$P_f = g(N_f) = \beta_3 N_f^3 + \beta_2 N_f^2 + \beta_1 N_f + \beta_0 \quad (6)$$

$$u = h(N_f) = \gamma_1 N_f + \gamma_0. \quad (7)$$

For this purpose, we vary the fan speed setpoint from the minimum value of 10% to the maximum value of 90% of the rated fan power (with a step of 5%) and record the air flow rate and electric power. Each setpoint is kept for 6 minutes, but the first 20 seconds of the data after each step change are discarded to account for communication delays and the fan transients. The identified parameters are given in Table 4, whereas the measurements and identified models are shown in Fig. 6. The fitting performance is very high: the RMSE is only 5 W for the speed-to-power model and 21 W for the flow-to-power model.

4 Level 1: Reserve Scheduler

4.1 Robust Reserve Scheduling Formulation

Let $R_{u,k}$ and $R_{d,k}$ denote the electric reserve capacities at time step k for regulation up and down, respectively.¹ It is convenient to define also the thermal up- and down-reserve capacities $r_{u,k}$ and $r_{d,k}$ as the maximum changes in the mass air flow rate due to reserve provision. In cooling operation, a request for regulation up results in a reduction in air mass flow rate, such that $R_{u,k}$ is related to $r_{d,k}$. On the other hand, regulation down results in an increase in air mass flow rate ($R_{d,k}$ is related to $r_{u,k}$). $R_{u,k}$ and $R_{d,k}$ are coupled to $r_{d,k}$ and $r_{u,k}$ with the flow-to-power fan model (5) according to

$$R_{u,k} = f(u_k) - f(u_k - r_{d,k}) \quad (8)$$

$$R_{d,k} = f(u_k + r_{u,k}) - f(u_k), \quad (9)$$

¹Up-reserve is an increase of generation or decrease of consumption, whereas down-reserve is a decrease of generation or increase of consumption.

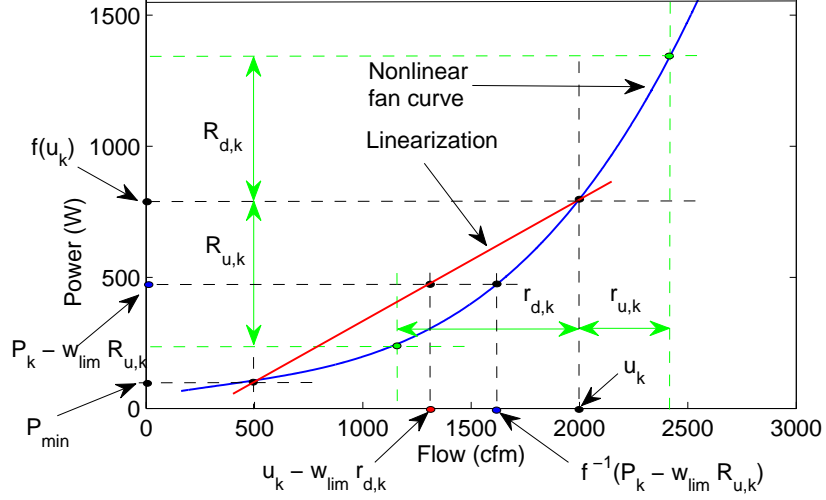


Figure 7: The fan curve linearization for the optimization. The thermal reserves and the electric reserves are shown around an air flow rate operating point.

where u_k is the operating point of air flow. This nonlinear relationship is graphically shown in Fig 7.

The objective is to minimize the total cost defined as the sum of energy consumption cost and reserve profit

$$c_k P_k + \lambda_k (R_{d,k} + R_{u,k}) , \quad (10)$$

where c_k is the electricity price and P_k is the fan power consumption. Assuming the same payment λ_k for up- and down-reserves and using (8) and (9), the reserve profit is given by

$$\lambda_k (R_{d,k} + R_{u,k}) = \lambda_k [f(u_k + r_{u,k}) - f(u_k - r_{d,k})]. \quad (11)$$

Typically, the TSO requests the reserve energy as a fraction of the reserve capacity using a normalized frequency regulation signal $w_k \in [-1, 1]$ [34]. Thus, the reserve at time step k is

$$R_k = \begin{cases} w_k R_{u,k}, & \text{if } w_k < 0 \\ w_k R_{d,k}, & \text{if } w_k \geq 0. \end{cases} \quad (12)$$

The electric reserve request can be translated to a perturbation around u_k using the fan curve

$$\Delta u_k = f^{-1}(P_k + R_k) - u_k . \quad (13)$$

With the above notation, the multi-period robust reserve scheduling problem

can be written as

$$\min_{u_k, r_{u,k}, r_{d,k}} \sum_{k=0}^{N_1-1} c_k f(u_k) - \lambda_k (R_{d,k} + R_{u,k}) \quad (14a)$$

$$\text{s.t. } x_{k+1} = Ax_k + B_u T_s \cdot (u_k + \Delta u_k) + B_{xu} x_k \cdot (u_k + \Delta u_k) + B_v v_k, \forall k \quad (14b)$$

$$u_{\min,1} \leq u_k + \Delta u_k \leq u_{\max,1}, \forall w_k \in [-1, 1], \forall k \quad (14c)$$

$$x_{\min,k} \leq x_k \leq x_{\max,k}, \forall w_k \in [-w_{\text{lim}}, w_{\text{lim}}], \forall k. \quad (14d)$$

Equation (14b) represents the building dynamics, whereas (14c) and (14d) set upper and lower bounds on the air mass flow rate and temperature, respectively. The limits $u_{\min,1}$ and $u_{\max,1}$ are calculated at the fan speeds 20% and 80% with

$$u_{\min,1} = h(20\%), \quad u_{\max,1} = h(80\%). \quad (15)$$

The comfort zone (temperature) limits $x_{\min,k}$ and $x_{\max,k}$ are time-varying and different for working and non-working hours.

Uncertainty in the unknown frequency regulation signal, w_k , is explicitly handled in the reserve scheduling problem. Formulation (14) builds robustness to w_k with the robust input and state constraints (14c) and (14d). Since the worst case in terms of power is either full up-reserve or down-reserve activation, w_k can take any value in $[-1, 1]$ in (14c). The energy content of the regulation signal over 15 minutes is typically limited, which is captured by the uncertainty set $w_k \in [-w_{\text{lim}}, w_{\text{lim}}]$ in (14d), where $0 < w_{\text{lim}} \leq 1$ is the energy limit.

4.2 Reformulation and Approximation

Due to the uncertain variable w_k , problem (14) is not directly solvable. However, we derive the robust counterpart problem (16) by formulating the input and state constraints of (14) only for the boundaries of the uncertainty w_k . In (16), \bar{x}_k and \underline{x}_k are the worst case higher and lower state trajectories, respectively. We show in Proposition 1 that problems (16) and (14) are equivalent, if the building operates in cooling mode.

$$\min_{u_k, r_{u,k}, r_{d,k}} \sum_{k=0}^{N_1-1} c_k f(u_k) - \lambda_k (R_{d,k} + R_{u,k}) \quad (16a)$$

$$\text{s.t. } \bar{x}_{k+1} = A\bar{x}_k + B_u T_s \cdot f^{-1}(P_k - w_{\text{lim}} R_{u,k}) + B_{xu} \bar{x}_k \cdot f^{-1}(P_k - w_{\text{lim}} R_{u,k}) + B_v v_k, \forall k \quad (16b)$$

$$\underline{x}_{k+1} = A\underline{x}_k + B_u T_s \cdot f^{-1}(P_k + w_{\text{lim}} R_{d,k}) + B_{xu} \underline{x}_k \cdot f^{-1}(P_k + w_{\text{lim}} R_{d,k}) + B_v v_k, \forall k \quad (16c)$$

$$u_{\min,1} \leq u_k - r_{d,k}, \quad u_k + r_{u,k} \leq u_{\max,1}, \forall k \quad (16d)$$

$$x_{\min,k} \leq \underline{x}_k, \quad \bar{x}_k \leq x_{\max,k} \quad \forall k. \quad (16e)$$

Lemma 1. *Function $f(u)$ is both monotonic and convex.*

Proof. It is sufficient to show that the 1st and 2nd order derivatives of f are non-negative for the parameters of Table 4. ■

Lemma 2. *If $w_k \in [-w_{lim}, w_{lim}]$ with $0 < w_{lim} \leq 1$, the following statements are true:*

$$\min_{w_k} (u_k + \Delta u_k) = f^{-1}(P_k - w_{lim} R_{u,k}) \text{ for } w_{lim} \leq 1 \quad (17)$$

$$\max_{w_k} (u_k + \Delta u_k) = f^{-1}(P_k + w_{lim} R_{d,k}) \text{ for } w_{lim} \leq 1 \quad (18)$$

$$\min_{w_k} (u_k + \Delta u_k) = u_k - r_{d,k}, \text{ for } w_{lim} = 1 \quad (19)$$

$$\max_{w_k} (u_k + \Delta u_k) = u_k + r_{u,k}, \text{ for } w_{lim} = 1. \quad (20)$$

Proof. The proof is given in Appendix A. ■

Assumption 1. *We assume that the building operates in cooling mode by deactivating the heating coil of the AHU, and the SAT is controlled to a setpoint T_s that satisfies*

$$T_s \leq x_{min,k} \leq T_{r,k}, \forall k. \quad (21)$$

Therefore, increasing the air flow rate will always decrease the room temperature.

Proposition 1. *Under Assumption 1, optimization problems (14) and (16) are equivalent.*

Proof. The proof is given in Appendix B. ■

The dynamics in (16) involve the inverse of a polynomial combination of optimization variables and are complex. This is in contrast to the formulations of [19–21] where the nonlinear fan dynamics were not considered. We propose to approximate (16) by the simple linearization of the inverse function shown in Fig. 7, which leads to problem (22). As shown by Propositions 2 and 3, problems (16) and (22) are equivalent only for the special case $w_{lim} = 1$, but not in general ($0 < w_{lim} \leq 1$).

$$\min_{u_k, r_{u,k}, r_{d,k}} \sum_{k=0}^{N_1-1} c_k f(u_k) - \lambda_k (R_{d,k} + R_{u,k}) \quad (22a)$$

$$\text{s.t. } \bar{x}_{k+1} = A\bar{x}_k + B_u T_s \cdot (u_k - w_{lim} \cdot r_{d,k}) + B_{xu} \bar{x}_k \cdot (u_k - w_{lim} \cdot r_{d,k}) + B_v v_k, \forall k \quad (22b)$$

$$\underline{x}_{k+1} = A\underline{x}_k + B_u T_s \cdot (u_k + w_{lim} \cdot r_{u,k}) + B_{xu} \underline{x}_k \cdot (u_k + w_{lim} \cdot r_{u,k}) + B_v v_k, \forall k \quad (22c)$$

(16d), (16e).

Proposition 2. Let \bar{x}_k^* and \underline{x}_k^* denote the maximum and minimum state trajectories of the original problem (16). Furthermore, let \bar{x}_k^* and \underline{x}_k^* denote the maximum and minimum state trajectories obtained by (22). With $0 < w_{lim} \leq 1$, $\bar{x}_k^* \geq \bar{x}_k^*$ and $\underline{x}_k^* \geq \underline{x}_k^*$ hold for any time step k , i.e., the approximation (22) overestimates the maximum and minimum room temperatures compared with the original problem (16).

Proof. The proof is given in Appendix C. ■

Proposition 3. Problems (16), (22) are equivalent if $w_{lim} = 1$.

Proof. The proof follows directly by rewriting (16b) and (16c) using (19), (20) and (32) from Lemma 2. ■

Note that the overestimation of the maximum and minimum room temperature builds additional robustness to temperature excursions above $x_{max,k}$, but it reduces robustness to temperature excursions below $x_{min,k}$. This is desirable because the state trajectory will generally remain closer to $x_{max,k}$ than $x_{min,k}$ due to minimization of energy consumption cost in (22a).

Problem (22) is a deterministic nonlinear optimization problem with cubic objective function, bilinear equality constraints and linear inequality constraints. Although this is a non-convex problem, it is possible to solve it in due time with the solver IPOPT due to its relatively small size (the problem was compiled with YALMIP [35]). The outcome of (22) is the up-reserve $R_{u,k}$ and down-reserve $R_{d,k}$ capacity for each time slot of the scheduling horizon $k \in [0, N_1 - 1]$.

4.3 Energy Limit of Regulation Signal

The energy limit w_{lim} of the regulation signal is the worst case normalized reserve request. To identify this limit, we analyze 2-month historical data of the RegD signal from the Pennsylvania, Jersey, and Maryland Power Market (PJM) (December 2012 to January 2013). Fig. 8 shows the cumulative distribution of the signal's energy content over 15 minute intervals, as well as the actual worst case, the median, 95%, 97.5%, and 99% percentiles. Since the actual worst case of $w_{lim} = 0.88$ would lead to very conservative solutions, we define the worst case as the 97.5% percentile of the distribution ($w_{lim} = 0.25$). Therefore, the requested reserve energy by RegD over 15 minutes will be less than 25% of the reserve capacity with probability 97.5%.

The worst case reserve request along the prediction horizon is obtained in (14d) by taking the worst case for each time step independently [19]. Although this is a conservative approach, it has the advantage of building additional robustness to modeling and forecast uncertainties.

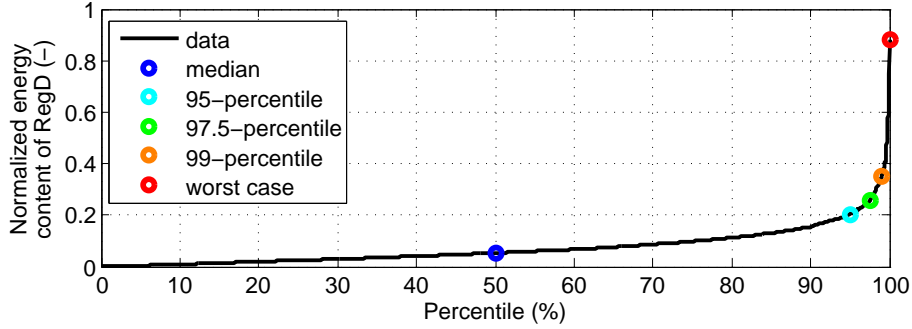


Figure 8: Cumulative distribution of RegD signal's energy content in 15 minutes.

4.4 Modeling Reserve Product Constraints

Problem (22) allows us to select different reserve capacities for each 15-min time slot, as well as different $R_{u,k}$ and $R_{d,k}$ for the same time slot. However, many markets have requirements on the structure of the reserve product, in particular reserve blocks with minimum duration and/or symmetric reserves.

Reserve blocks with minimum duration of $T_{\text{res}} \in \mathbb{N}$ time steps can be modeled by adding in (22) the constraints $R_{u,k} = R_{u,k+j}$ and $R_{d,k} = R_{d,k+j} \forall k = nT_{\text{res}} + 1, \forall j \in \{1, \dots, T_{\text{res}}\}$, where $n \in \mathbb{N}$ and $n \leq (N_1 - 1)/T_{\text{res}}$. We select $T_{\text{res}} = 4$ to require the reserve capacities to be constant over periods of 1 hour.

Symmetric reserve capacities can be enforced by introducing in (22) the constraint $R_{u,k} = R_{d,k} \forall k$, and are expected to reduce the amount of reserves due to the nonlinear flow-to-power fan model. In addition, symmetric reserves and/or reserve blocks with minimum duration increase the complexity because they are nonlinear equality constraints on $r_{u,k}$ and $r_{d,k}$.

Even if symmetric electric reserve capacities are not required from the resources, we chose to impose symmetry in the thermal domain to limit the impact of offering reserves on the room temperature. If the thermal reserves are symmetric, the electric reserves will be asymmetric due to the nonlinear fan curve and (8), (9). In this case, a single variable r_k can replace $r_{u,k}$ and $r_{d,k}$, which is expected to reduce the computation time. We term this type of reserve offering as “*asymmetric*” operation.

5 Level 2: Room Climate Controller

5.1 MPC Formulation

The level 2 controller determines the air mass flow rate setpoint u_k with the robust MPC formulation

$$\min_{u_k, r_{u,k}, r_{d,k}} \sum_{k=0}^{N_2-1} c_k f(u_k) \quad (23a)$$

$$u_{\min,2} \leq u_k - r_{d,k}, \quad u_k + r_{u,k} \leq u_{\max,2}, \quad \forall k \quad (23b)$$

$$R_{u,k}^* = f(u_k) - f(u_k - r_{d,k}), \quad \forall k \quad (23c)$$

$$R_{d,k}^* = f(u_k + r_{u,k}) - f(u_k), \quad \forall k \quad (23d)$$

$$(16e), (22b), (22c) .$$

Problem (23) is similar to (22) with the main differences being (i) the electric reserve capacities $R_{u,k}^*$ and $R_{d,k}^*$ are fixed from level 1, and (ii) the only objective is to minimize energy cost.

The MPC selects u_k , $r_{u,k}$ and $r_{d,k}$ such that the electric reserves $R_{u,k}^*$ and $R_{d,k}^*$ can be provided according to constraints (23c) and (23d). Weather forecasts are used in (23) and are updated at every time step. The comfort constraints of (22) and (23) are modeled as soft constraints with high penalties to avoid infeasibility due to plant-model mismatch or forecast errors.

The upper and lower bounds on the air flow rate $u_{\min,2}$ and $u_{\max,2}$ of the MPC are less tight than those of the reserve scheduler to facilitate meeting the comfort zone constraints

$$u_{\min,2} = h(10\%), \quad u_{\max,2} = h(90\%) . \quad (24)$$

The selected bounds correspond to the minimum acceptable fan speed values suggested by the building manager of FLEXLAB.

5.2 Kalman Filter

Since $T_{m,k}$ is not measured directly and the measurement of $T_{r,k}$ is noisy, we use an extended Kalman filter to obtain a state estimate \hat{x}_k for the MPC and the reserve scheduler.

Assuming additive process and measurement noise, the a priori error covariance $P_{e,k}^-$, a posteriori error covariance $P_{e,k}$ and Kalman gain K_k are given by [36]

$$P_{e,k}^- = F_k P_{e,k} F_k^\top + Q \quad (25)$$

$$K_k = P_{e,k}^- H_k^\top (H_k P_{e,k}^- H_k^\top + R)^{-1} \quad (26)$$

$$P_{e,k} = (I - K_k H_k) P_{e,k}^- , \quad (27)$$

where F_k is the Jacobian matrix of system dynamics and H_k is the Jacobian matrix of the output $y_k = Cx_k$; $Q = [0.4 \ 0; \ 0 \ 0.4]$ and $R = 0.1$ are the process and

measurement noise covariance matrices, respectively;² and I is the identity matrix. Let ϕ_x denote the partial derivative of bilinear dynamics and φ_x denote the partial derivative of the output equation, both with respect to the state x_k . The matrices F_k and H_k are calculated with

$$F_k = \phi_x(\hat{x}_{k-1}, u_{k-1}) = A + B_{xu}\hat{x}_{k-1}u_{k-1} \quad (28)$$

$$H_k = \varphi_x(\hat{x}_{k-1}, u_{k-1}) = C. \quad (29)$$

6 Level 3: Frequency Regulation Controller

Level 3 controls the fan speed (input of the fan controller) such that the fan power tracks the frequency regulation signal. Our approach is different from [26] that used the frequency of the VFD as a control variable, and from [24] where a fan speed command was superimposed on the output of the fan controller.

There are four requirements for the frequency regulation controller: fast response, minimal computation effort, accuracy and stability. For this purpose, we developed a novel switched controller with two loops: (i) Ctrl1: a model-based, feedforward controller, and (ii) Ctrl2: a model-free, feedback PI controller. The feedforward controller uses the static speed-to-power fan model (6) and it is inherently stable due to the absence of feedback. The PI controller is used to reduce the steady-state error of the feedforward controller, but its stability is not guaranteed and requires gain tuning. The discrete-time implementation of the switched controller is described by Algorithm 1.

Step 3 of Algorithm 1 uses the flow-to-power fan model (5) to translate the scheduled flow rate of level 2 to baseline power consumption. The desired fan power P_d is computed at step 5 based on the baseline, the reserve capacity of level 1 and the regulation signal. The new control error e_{new} is calculated at step 8 as the difference between P_d and the measured fan power P_f . At step 9 the condition $|e_{\text{new}}| \leq \varepsilon$ is checked to decide whether Ctrl1 or Ctrl2 will be used (ε is a tolerance that represents the fan model's accuracy). If $|e_{\text{new}}| \leq \varepsilon$ holds, then we activate Ctrl2 (the PI controller's discrete time implementation is given from step 10 to step 13). On the other hand, if $|e_{\text{new}}| > \varepsilon$, we activate Ctrl1 and determine the fan speed at step 15 according to (6).

After a large power setpoint change, Ctrl1 remains active for as long as $|e_{\text{new}}|$ is larger than ε , whereas the controller switches to Ctrl2 when $|e_{\text{new}}| \leq \varepsilon$. When we switch from Ctrl1 to Ctrl2, we reset the integral error to zero (step 16 of Algorithm 1) to avoid large overshoots due to accumulated errors. Furthermore, if the output of Ctrl2 is larger than 90% or smaller than 10%, we cap or floor the fan speed to these values.

²We set $R = 0.1$ based on the accuracy of the temperature sensors. Based on the building model's RMSE (equal to 0.42°C from Table 1), an initial estimate of the diagonal entries of Q is $0.42^2 = 0.1764$. We chose the larger value 0.4 because the model's out-of-sample RMSE will be higher than 0.42.

Algorithm 1 Implementation of the switched controller

```
1: initialize old tracking error  $e_{\text{old}} = 0$  and fan speed  $N_f$ 
2: while experiment is running do
3:   calculate baseline power:  $P_s = f(\dot{m}_s)$ 
4:   compute reserve:  $R = wR_d$  (if  $w > 0$ ),  $R = wR_u$  (if  $w \leq 0$ )
5:   calculate desired fan power:  $P_d = P_s + R$ 
6:   repeat
7:     measure fan power  $P_f$ 
8:     calculate new tracking error:  $e_{\text{new}} = P_d - P_f$ 
9:     if  $|e_{\text{new}}| \leq \varepsilon$  then
10:      set PI output:  $N_{f,\text{pi}} = N_f + K_p(e_{\text{new}} - e_{\text{old}}) + K_i \Delta t e_{\text{new}}$ 
11:      cap fan speed:  $N_f = \min[\max(N_{f,\text{pi}}, N_{f,\text{min}}), N_{f,\text{max}}]$ 
12:      set fan speed to  $N_f$ 
13:      set old tracking error to:  $e_{\text{old}} = e_{\text{new}}$ 
14:     else
15:       set fan speed to:  $N_f = g(P_d)$ 
16:       set old tracking error to:  $e_{\text{old}} = 0$ 
17:     end if
18:   until elapsed time is equal to control loop duration
19: end while
```

Table 5: Tuned gains of the PI controller

Region (kW)	[0, 0.5)	[0.5, 1)	[1, 1.5)	[1.5, 2)	[2, 2.5)
K_p (proportional)	0.004	0.004	0.004	0.0045	0.004
K_i (integral)	0.01	0.0035	0.003	0.0025	0.002

Due to the nonlinear fan curve, gain scheduling was used in the PI controller. Five operating regions were defined and different proportional (K_p) and integral gains (K_i) were calculated for each region using the Ziegler-Nichols method [37]. We performed step response tests with $K_i = 0$ and gradually increased K_p until a critical value with stable and consistent oscillations in fan power. The critical proportional gain and the period of oscillations are used to determine K_p and K_i .

The gains obtained with the Ziegler-Nichols method served as an initial guess, whereas the final gains were determined with trial and error and are presented in Table 5. The K_p gains are lower and the K_i gains are higher than those suggested by the Ziegler-Nichols method because the goal of the PI controller (Ctrl2) is to correct the steady-state error of Ctrl1, but not to recover the system after a large setpoint change.

The proposed switched controller is advantageous in terms of stability and performance compared with the open-loop controller of [26] and the closed-loop controller of [24]. Ctrl1 allows us to track sudden power setpoint changes without the need of high gains in Ctrl2 that would compromise stability.

7 Conclusion and Outlook

In Part I of this two-part paper, we presented the commercial building test facility FLEXLAB for a frequency regulation demonstration project. We developed and compared different building models for use in a day-ahead reserve scheduler and an MPC for building climate control. Specifically, we presented mathematical reformulations to include the nonlinear fan dynamics in the optimization problems. Furthermore, we proposed a switched controller for frequency regulation that is accurate and inherently stable. In Part II we report extensive experimental results using the developed models and controllers.

A Proof of Lemma 2

Proof. From the definition of Δu_k in (13) and (12) we get

$$\min_{w_k} (u_k + \Delta u_k) = \min_{w_k \in [-w_{\text{lim}}, 0)} [f^{-1}(P_k + w_k R_{u,k})]. \quad (30)$$

Due to monotonicity, $\operatorname{argmin}[f^{-1}(P_k + w_k R_{u,k})]$ is equal to

$$\operatorname{argmin}(P_k + w_k R_{u,k}) = -w_{\text{lim}}. \quad (31)$$

Substituting the minimizer $-w_{\text{lim}}$ in (30) we get (17). Equation (19) is a special case of (17) derived as

$$\begin{aligned} f^{-1}(P_k - w_{\text{lim}} R_{u,k}) &= f^{-1}[f(u_k) - R_{u,k}] = \\ f^{-1}[f(u_k) - f(u_k) + f(u_k - r_{d,k})] &= u_k - r_{d,k}, \end{aligned} \quad (32)$$

where (8) is used. The maximization case for (18) and (20) can be proved analogously but the proof is omitted for brevity. ■

B Proof of Proposition 1

Proof. It is sufficient to show that the input constraints (16d) are equivalent to (14c), and that the set of state constraints (16b), (16c) and (16e) is equivalent to the set of constraints (14b) and (14d). The equivalence of input constraints follows directly from (19) and (20). For the state constraints we first write (14b) as

$$x_{k+1} = Ax_k + (B_u T_s + B_{xu} x_k) \cdot (u_k + \Delta u_k) + B_v v_k. \quad (33)$$

Constraint (14d) is applied only to the first state $T_{r,k} = Cx_k$ of the state vector x_k , where $C = [1 \ 0]$ is the output matrix. Observing that $CB_u T_s = bT_s$ and $CB_{xu} x_k = -bT_{r,k}$, constraint (14d) can be written as

$$\min_{w_k} [CAx_k + b(T_s - T_{r,k}) \cdot (u_k + \Delta u_k) + CB_v v_k] \geq x_{\min,k} \quad (34)$$

$$\max_{w_k} [CAx_k + b(T_s - T_{r,k}) \cdot (u_k + \Delta u_k) + CB_v v_k] \leq x_{\max,k}. \quad (35)$$

Due to assumption 1, we have $b(T_s - T_{r,k}) \leq 0$ and so the left hand side of (34) is minimized when $u_k + \Delta u_k$ is maximized. From (18), this is achieved when $u_k + \Delta u_k = f^{-1}(P_k + w_{\text{lim}}R_{d,k})$ holds. Let \underline{x}_k denote the minimum state trajectory at time step k . The time evolution of \underline{x}_k is therefore obtained by $\underline{x}_{k+1} = CA\underline{x}_k + b(T_s - C\underline{x}_k) \cdot f^{-1}(P_k + w_{\text{lim}}R_{d,k}) + CB_v v_k$, which is essentially (16c). Thus, if $x_{\text{min},k} \leq \underline{x}_k$ holds, then the left hand side of (14d) also holds because $x_k \leq \underline{x}_k \forall w_k$.

Analogous arguments can be used to show that (35) results in (16b) and $\bar{x}_k \leq x_{\text{max},k}$, which are equivalent to the right hand side of (14d), but this is omitted for brevity. ■

C Proof of Proposition 2

Proof. Using definition (8) and the convexity of f we get

$$\begin{aligned} P_k - w_{\text{lim}}R_{u,k} &= f(u_k) - w_{\text{lim}}[f(u_k) - f(u_k - r_{d,k})] \\ &= (1 - w_{\text{lim}})f(u_k) + w_{\text{lim}}f(u_k - r_{d,k}) \\ &\geq f[(1 - w_{\text{lim}})u_k + w_{\text{lim}}(u_k - r_{d,k})]. \end{aligned} \quad (36)$$

Using the monotonicity of f in (36) we get

$$\begin{aligned} f^{-1}(P_k - w_{\text{lim}}R_{u,k}) &\geq (1 - w_{\text{lim}})u_k + w_{\text{lim}}(u_k - r_{d,k}) \\ &= u_k - w_{\text{lim}}r_{d,k}. \end{aligned} \quad (37)$$

$\bar{x}_k^* \geq \underline{x}_k^*$ is now obtained by combining (37), (16b), (22b), and using the same arguments related to $b(T_s - T_{r,k}) \leq 0$ as in the proof of Proposition 1. Similarly, one can show that $u_k + w_{\text{lim}}r_{u,k} \leq f^{-1}(P_k + w_{\text{lim}}R_{d,k})$ holds and so that $\underline{x}_k^* \geq \bar{x}_k^*$ also holds. Fig. 7 provides a graphical interpretation of (37). ■

References

- [1] Y. Makarov, C. Loutan, J. Ma, P. De Mello, Operational impacts of wind generation on California power systems, *IEEE Transactions on Power Systems* 24 (2) (2009) 1039–1050.
- [2] F. Schweppe, R. Tabors, J. Kirtley Jr, H. Outhred, F. Pickel, A. Cox, Homeostatic utility control, *IEEE Transactions on Power Apparatus and Systems* PAS-99 (3) (1980) 1151–1163.
- [3] H. Hao, T. Middelkoop, P. Barooah, S. Meyn, How demand response from commercial buildings will provide the regulation needs of the grid, in: *50th Annual Allerton Conference on Communication, Control, and Computing*, Monticello, Illinois, USA, 2012.
- [4] Buildings energy data book, Available online at <http://buildingsdatabook.eren.doe.gov/default.aspx>.

- [5] J. A. Crabb, N. Murdoch, J. M. Penman, A simplified thermal response model, *Building Services Engineering Research and Technology* 8 (1) (1987) 13–19.
- [6] R. Kramer, J. van Schijndel, H. Schellen, Simplified thermal and hygric building models: a literature review, *Frontiers of Architectural Research* 1 (4) (2012) 318–325.
- [7] J. E. Braun, Reducing energy costs and peak electrical demand through optimal control of building thermal storage, *ASHRAE Transactions* 96 (2) (1990) 876–887.
- [8] F. B. Morris, J. E. Braun, S. J. Treado, Experimental and simulated performance of optimal control of building thermal storage, *ASHRAE Transactions* 100 (1) (1994) 402–414.
- [9] G. P. Henze, R. H. Dodier, M. Krarti, Development of a predictive optimal controller for thermal energy storage systems, *HVAC&R Research* 3 (3) (1997) 233–264.
- [10] S. Kiliccote, Open automated demand response communications in demand response for wholesale ancillary services, Lawrence Berkeley National Laboratory.
- [11] B. Kirby, J. Kueck, T. Laughner, K. Morris, Spinning reserve from hotel load response, *The Electricity Journal* 21 (10) (2008) 59–66.
- [12] D. H. Blum, L. K. Norford, Dynamic simulation and analysis of ancillary service demand response strategies for variable air volume HVAC systems, *HVAC&R Research* 20 (8) (2014) 908–921.
- [13] P. Kundur, *Power system stability and control*, Edited by N. J. Balu and M. G. Lauby, New York: McGraw-hill, 1994.
- [14] S. Kawachi, H. Hagiwara, J. Baba, Modeling and simulation of heat pump air conditioning unit intending energy capacity reduction of energy storage system in microgrid, in: *European Conference on Power Electronics and Applications*, Birmingham, UK, 2011.
- [15] P. Zhao, G. P. Henze, S. Plamp, V. J. Cushing, Evaluation of commercial building HVAC systems as frequency regulation providers, *Energy and Buildings* 67 (2013) 225–235.
- [16] H. Hao, A. Kowli, Y. Lin, P. Barooah, S. Meyn, Ancillary service for the grid via control of commercial building HVAC systems, in: *American Control Conference (ACC)*, Washington DC, USA, 2013.

- [17] Y. Lin, P. Barooah, S. Meyn, Low-frequency power grid ancillary services from commercial building HVAC systems, in: IEEE SmartGridComm Conference, Vancouver, Canada, 2013.
- [18] M. Maasoumy, C. Rosenberg, A. Sangiovanni-Vincentelli, D. S. Callaway, Model predictive control approach to online computation of demand-side flexibility of commercial buildings HVAC systems for supply following, in: ACC, Portland, USA, 2014.
- [19] E. Vrettos, F. Oldewurtel, F. Zhu, G. Andersson, Robust provision of frequency reserves by office building aggregations, in: World Congress of the International Federation of Automatic Control (IFAC), Cape Town, South Africa, 2014.
- [20] E. Vrettos, F. Oldewurtel, G. Andersson, Robust energy-constrained frequency reserves from aggregations of commercial buildings, IEEE Transactions on Power Systems (early access).
- [21] E. Vrettos, G. Andersson, Scheduling and provision of secondary frequency reserves by aggregations of commercial buildings, IEEE Transactions on Sustainable Energy 7 (2) (2016) 850–864.
- [22] G. S. Pavlak, G. P. Henze, V. J. Cushing, Optimizing commercial building participation in energy and ancillary service markets, Energy and Buildings 81 (2014) 115–126.
- [23] J. T. Hughes, A. D. Dominguez-Garcia, K. Poolla, Identification of virtual battery models for flexible loads, IEEE Transactions on Power Systems (early access).
- [24] Y. Lin, P. Barooah, S. Meyn, T. Middelkoop, Experimental evaluation of frequency regulation from commercial building HVAC system, IEEE Transactions on Smart Grid 6 (2) (2015) 776–783.
- [25] S. Kiliccote, et al., Field testing of automated demand response for integration of renewable resources in California’s ancillary services market for regulation products, Tech. rep., LBNL (2007).
- [26] J. MacDonald, S. Kiliccote, J. Boch, J. Chen, R. Nawy, Commercial building loads providing ancillary services in PJM, in: ACEEE Summer Study on Energy Efficiency in Buildings, Pacific Grove, USA, 2014.
- [27] Y. Kim, E. Fuentes, L. K. Norford, Experimental study of grid frequency regulation ancillary service of a variable speed heat pump, IEEE Transactions on Power Systems (to appear).

- [28] L. Su, L. K. Norford, Demonstration of HVAC chiller control for power grid frequency regulation – Part 1: Controller development and experimental results, *Science and Technology for the Built Environment* 21 (8) (2015) 1134–1142.
- [29] L. Su, L. K. Norford, Demonstration of HVAC chiller control for power grid frequency regulation – Part 2: Discussion of results and considerations for broader deployment, *Science and Technology for the Built Environment* 21 (8) (2015) 1143–1153.
- [30] I. Biel, I. Hiskens, S. Backhaus, Round-trip efficiency of fast demand response in a large commercial air conditioner, *Energy and Buildings* 97 (2015) 47–55.
- [31] E. Vrettos, E. C. Kara, J. MacDonald, G. Andersson, D. Callaway, Experimental demonstration of frequency regulation by commercial buildings – Part II: Results and performance evaluation, available at [arXiv.org](https://arxiv.org).
- [32] Survey on ancillary services procurement and electricity balancing market design, Available at www.entsoe.eu/publications/position-papers.
- [33] J. Široký, F. Oldewurtel, J. Cigler, S. Prívvara, Experimental analysis of model predictive control for an energy efficient building heating system, *Applied Energy* 88 (9) (2011) 3079–3087.
- [34] Basic principles of ancillary service products, Available online at www.swissgrid.ch, last accessed on 23.01.2015.
- [35] J. Löfberg, Yalmip: A toolbox for modeling and optimization in MATLAB, in: *IEEE International Symposium on Computer Aided Control Systems Design*, Taipei, Taiwan, 2004, pp. 284–289.
- [36] G. Welch, G. Bishop, *An introduction to the Kalman filter*. 2006, University of North Carolina: Chapel Hill, North Carolina, US.
- [37] J. G. Ziegler, N. B. Nichols, Optimum settings for automatic controllers, *ASME Transactions* 64 (11) (1942) 759–765.